PCCP

PAPER

View Article Online
View Journal | View Issue

Cite this: *Phys. Chem. Chem. Phys.*, 2019, **21**, 9310

Topological Dirac states in transition-metal monolayers on graphyne†

Kai Wang, ‡[a] Yun Zhang, ‡[b] Wei Zhao, [c] Ping Li, [a] Jian-Wen Ding,[a] Guo-Feng Xie[d] and Zhi-Xin Guo*[e]

Received 27th February 2019,
Accepted 5th April 2019

DOI: 10.1039/c9cp01153f

rsc.li/pccp

Realizing topological Dirac states in two-dimensional (2D) magnetic materials is particularly important to spintronics. Here, we propose that such states can be obtained in a transition-metal (Hf) monolayer grown on a 2D substrate with hexagonal hollow geometry (graphyne). We find that the significant orbital hybridizations between Hf and C atoms can induce sizable magnetism and bring three Dirac cones at/around each high-symmetry $K(K')$ point in the Brillouin zone. One Dirac cone is formed by pure spin-up electrons from the d_{z^2} orbital of Hf, and the remaining two are formed by crossover between spin-up electrons from the d_{z^2} orbital and spin-down electrons from the hybridization of the d_{xy/x^2-y^2} orbitals of Hf atoms and the p_z orbital of C atoms. We also find that the spin–orbit coupling effect can open sizable band gaps for the Dirac cones. The Berry curvature calculations further show the nontrivial topological nature of the system with a negative Chern number $C = -3$, which is mainly attributed to the Dirac states. Molecular dynamics simulations confirm the system's thermodynamic stability approaching room temperature. The results provide a new avenue for realizing the high-temperature quantum anomalous Hall effect based on 2D transition-metals.

1. Introduction

Since the experimental observation of monolayer (ML) hexagonal graphene,[1] 2D Dirac cone materials, characterized by linear band dispersion at K and K' points in the Brillouin zone (BZ), have attracted intense attention due to their unique physical properties and potential applications in nanoscale devices.[2–4] In the presence of spin–orbit coupling (SOC), the Dirac band can be encoded with a nontrivial band topology, which can exhibit either a quantum spin Hall (QSH) state or a quantum anomalous Hall (QAH) state depending on the time-reversal symmetry.[5,6]

The QSH effect in 2D materials was first predicted to exist in the p_z orbital of graphene[7] and then verified in other group-IV 2D monolayers, *i.e.*, silicene, germanene, and stanene.[8–11] It was later found that the $p_{x/y}$ orbitals can also induce the QSH effect but with a much larger band gap owing to the strong on-site SOC interactions in 2D materials such as X-hydride/halide, PbH monolayers, and the substrate-supported Bi monolayers.[11–14] In particular, the high-temperature QSH state had been recently experimentally observed in such a Bi monolayer on SiC.[15]

Despite the tremendous achievement in the QSH effect in 2D materials, realizing the QAH effect beyond the ultra-low temperature in 2D materials is still a challenge. The realization of the QAH effect in a system combines several basic ingredients: (1) the existence of an insulating bulk phase, (2) the breaking of time-reversal symmetry with finite magnetic ordering, and (3) the existence of a nonzero Chern number in the valence electrons. The conventional way to the QAH effect is *via* doping transition-metal (denoted as TM) atoms into the topological insulators, while the QAH effect can only exist at ultra-low temperature. Inspired by the discovered QSH effect in many p-electron 2D Dirac materials, recently great efforts have been made in the creation and discovery of d-electron 2D Dirac materials with robust magnetism, which may have potential to realize the room-temperature QAH effect.[16–20] Nevertheless, as far as we know, although several candidates had been theoretically proposed, none of them have been experimentally realized due to their rigorous requirement in the synthesis.

Here we propose a new strategy, *i.e.*, growing a TM ML on a 2D substrate with hexagonal hollow geometry, which is illustrated in the Hf ML on graphyne (a recently synthetized 2D carbon

[a] *Department of Physics and Institute for Nanophysics and Rare-earth Luminescence, Xiangtan University, Xiangtan 411105, China*
[b] *Department of Physics and Information Technology, Baoji University of Arts and Sciences, Baoji 721016, China*
[c] *School of Mechanical Engineering, Xiangtan University, Xiangtan, Hunan 411105, China*
[d] *Hunan Provincial Key Laboratory of Advanced Materials for New Energy Storage and Conversion, Hunan University of Science and Technology, Xiangtan, Hunan 411201, China*
[e] *Center for Spintronics and Quantum Systems, State Key Laboratory for Mechanical Behavior of Materials, School of Materials Science and Engineering, Xi'an Jiaotong University, Xi'an, Shaanxi, 710049, China. E-mail: zxguo08@xjtu.edu.cn*

† Electronic supplementary information (ESI) available. See DOI: 10.1039/c9cp01153f

‡ These authors contributed equally to this work.

allotrope of similar symmetry to graphene[21]). We find that the deposited Hf atoms prefer to locate on the hollow site of graphyne, which finally form a perfect honeycomb overlayer. This feature makes the Hf ML have three Dirac cones at/around the $K(K')$ BZ point near the Fermi level (E_F). One Dirac cone is formed by pure spin-up electrons from the d_{z^2} orbital of Hf and the remaining two are formed by the crossover of spin-up electrons from the d_{z^2} orbital and spin-down electrons from the hybridization of the d_{xy/x^2-y^2} orbitals of Hf and the p_z orbital of C (denoted as d_{hc} hybridization). We also find that the SOC can further open sizable band gaps for the Dirac cones. The Berry curvature calculations further show that the system is topologically nontrivial with a large negative Chern number $C = -3$.

2. Computational details

The total-energy electronic-structure calculations have been performed using density-functional theory (DFT) using the VASP code.[22,23] The ion–electron interaction was treated by the projector augmented-wave (PAW) technique. Exchange–correlation energies were taken into account by the generalized gradient approximation (GGA) using the Perdew–Burke–Ernzerhof functional.[24] The wave functions were constructed by using the PAW[25,26] approach with a plane wave cutoff energy of 500 eV. To obtain a more reliable calculation for the electronic band structure, the screened Heyd–Scuseria–Ernzerhof hybrid functional method (HSE06)[27,28] with mixing constant 1/4 was used. The effect of SOC is included self-consistently in the electronic structure calculations. The atomic positions and cell parameters were optimized using a conjugate gradient method with criteria of energy and Hellmann–Feynman force convergence being less than 10^{-5} eV per unit cell and 0.01 eV Å^{-1}, respectively. A sufficiently large vacuum of around 15 Å was adopted along the direction perpendicular to the surface (z axis) to avoid interaction between the Hf layer and its periodic images. A $15 \times 15 \times 1$ gamma centered k-point mesh was used to sample the BZ.[29]

With regard to the topological property calculations, we first used the maximally localized Wannier functions (MLWFs) to fit the band structures obtained from DFT calculations. Then the Berry curvature was calculated by using the WANNIER90 package.[30,31] The topological properties were calculated by using the software package WannierTools.[32]

3. Results and discussion

As shown in Fig. 1, graphyne consists of hexagonal carbon rings and acetylene linkages with a similar symmetry to graphene. A unit cell of graphyne contains 12 C atoms, with 6 C atoms forming the $C_{sp}{\equiv}C_{sp}$ hybridization and the remaining 6 C atoms forming the C_{sp^2}–C_{sp} hybridization, respectively. Our DFT calculations show that the optimized lattice constant is 6.890 Å, the C–C bond length within the hexagon is 1.425 Å, and the C_{sp^2}–C_{sp} and $C_{sp}{\equiv}C_{sp}$ bond lengths in the acetylenic links are 1.408 Å and 1.223 Å, respectively. These results agree well with previous studies.[33,34]

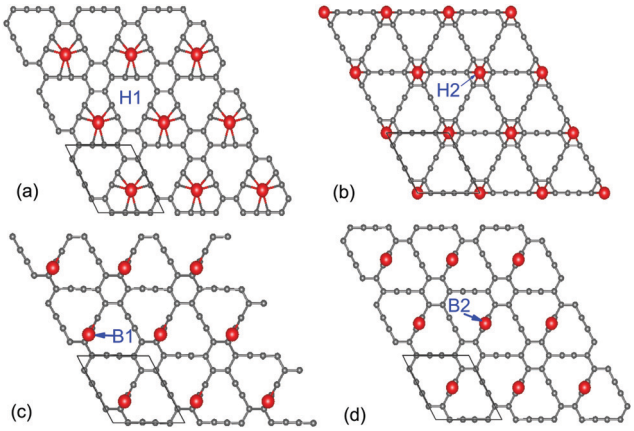

Fig. 1 Top view of the optimized configurations of Hf atoms on graphyne at H1 (a), H2 (b), B1 (c) and B2 (d) sites with 0.5 monolayer coverage, respectively. The red and gray balls denote Hf and C atoms, respectively. The black lines outline the primitive cell.

To identify the configuration of Hf atoms on graphyne (denoted as Hf–graphyne), we first explored the most preferred position for a single Hf atom depositing onto a graphyne primitive cell, which corresponds to 0.5 ML coverage of 2D Hf on graphyne. Four typical adsorption sites were considered, namely, H1 (a hollow site above the center of the acetylenic ring), H2 (a hollow site above the center of the hexagonal ring), B1 (a bridge site between the C_{sp^2} atom in the hexagonal ring and the C_{sp} atom in the acetylenic linkage), and B2 (a bridge site over the two C_{sp} atoms in the acetylenic linkage) sites, and their optimized atomic structures are shown in Fig. 1.

We further calculated the binding energy (E_b) of the four adsorption configurations, with E_b defined as

$$E_b = (E_{graphyne} + N_{Hf}\mu_{Hf} - E_{tot})/N_{Hf} \quad (1)$$

where $E_{graphyne}$ and E_{tot} are the total energies of graphyne and Hf–graphyne, respectively. N_{Hf} is the number of Hf atoms deposited on graphyne and μ_{Hf} is the chemical potential of Hf which is adopted as the total energy of an isolated Hf atom. The binding energy defined above is the energy gain to place Hf atoms onto the graphyne surface. As shown in Table 1, large positive E_b is obtained for all the four possible adsorption sites, indicating the exothermic reaction for the deposition of Hf atoms on graphyne. All the binding energies of the four configurations are larger than 2.5 eV per Hf atom, showing the strong chemical-interaction nature between Hf and graphyne. This feature is confirmed by the shortest Hf–C distances (L_{Hf-C}) in the four configurations (Table 1), which are in the range of

Table 1 The binding energy E_b and the shortest Hf–C distances (L_{Hf-C}) of typical Hf–graphyne structures with different coverages

	Adsorption site						
	0.5 ML coverage				1 ML coverage		
	H1	H2	B1	B2	H1–H1	H1–H2	H1–B1
E_b (eV)	4.730	2.809	3.222	2.602	4.674	4.376	4.208
L_{Hf-C} (Å)	2.216	2.356	2.178	2.184	2.318	2.243	2.054

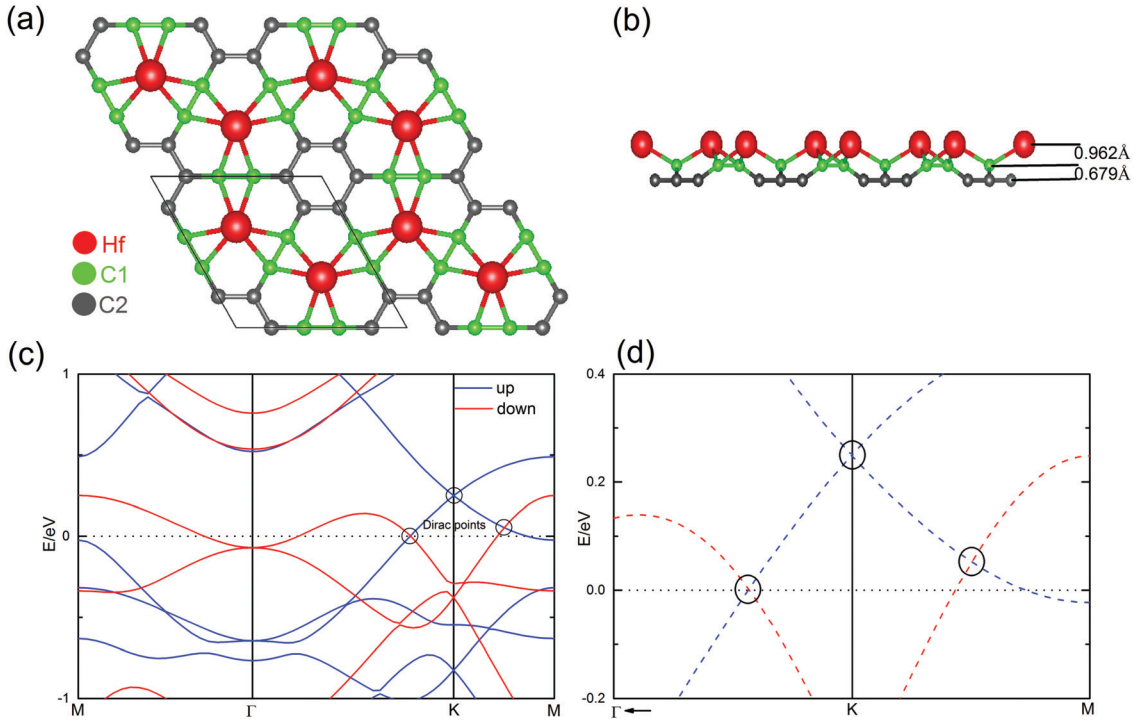

Fig. 2 Top view (a) and side view (b) of Hf–graphyne of the H1–H1 configuration. The red balls denote Hf atoms. The green and gray balls denote two types of carbon atoms, *i.e.*, C1 (high) and C2 (low) on the surface layer, respectively. The black lines in (a) outline the primitive cell. (c) The calculated band structure of Hf–graphyne, where the three Dirac cones are circled by black lines. (d) The enlarged band structure of (c) around the *K* point with higher precision.

2.18–2.36 Å, comparable to the sum of the covalent atomic radii (2.21 Å) of Hf and C atoms. The results show that the H1 configuration is most likely formed during the growth of 0.5 ML Hf on graphyne.

Then we considered the configuration for the deposition of an additional Hf atom onto the primitive cell of graphyne, which corresponds to the case of Hf coverage increasing from the 0.5 ML to 1.0 ML. Three possible adsorption sites (H1, H2, and B1) were considered for the additional Hf atom depositing on graphyne (the B2 site was also considered, but a structure satisfying convergence criterion was not found), where the optimized structures are shown in Fig. 2 and Fig. S1 (ESI†) for the H1–H1 and H1–H2/B1 configurations, respectively. It is found that the adsorption on the H1 site is more energetically favorable than that on H2 and B2 sites by 0.29–0.46 eV per Hf atom (Table 1). This means that when 1 ML Hf is grown on graphyne, all the Hf atoms prefer to locate on the hollow sites and thus form a honeycomb geometry like graphene (red balls in Fig. 2).

Note that the binding energies for both the 0.5 ML and 1 ML depositions of Hf on graphyne with the H1 site are larger than 4.6 eV per Hf atom, considerably larger than that of the Hf ML on Ir(111) (0.57 eV per Hf atom) which had been experimentally synthesized.[35] This result suggests that graphyne is an ideal substrate for the growth of a 2D Hf ML with hexagonal geometry. The improved binding energy between Hf atoms and graphyne is attributed to the presence of the more active sp hybridized C atoms in the graphyne sheet.[36] Such hybridization enables the π/π^* orbitals to easily rotate in any direction perpendicular to the line of –C≡C– bonds, and thus makes them strongly hybridize with the 5d/6s orbitals of the adsorbed Hf atoms in an acetylenic ring. As a result, the valence electrons of the Hf atoms not only couple with the $p_{x/y}$ orbitals but also with the p_z orbtials of C atoms in graphyne, leading to a strong interface interaction between the Hf ML and graphyne.[37]

We also performed *ab initio* molecular dynamics (AIMD) simulations to estimate the thermodynamic stability of Hf–graphyne since the graphyne surface severely distorted from the original structure, as shown in Fig. 2(a and b). AIMD simulations with canonical ensemble (*NVT*) were performed at a temperature of 300 K with a time step of 1 fs in 5 ps. A supercell containing 4 × 4 unit cells was adopted as the model. The total energy fluctuations during AIMD simulations and structure snapshots of Hf–graphyne taken at the end of 300 K simulation are shown in Fig. 3. The results show that Hf–graphyne can maintain its structural integrity even up to 300 K, indicating that Hf–graphyne has good stability approaching room temperature.

In the following, our discussions are focused on the most stable configuration of 1 ML Hf on graphyne, *i.e.*, the H1–H1 structure. Fig. 2(a) shows the top view of the H1–H1 structure, from which one can see that each Hf atom covalently bonds to its 6 nearest neighboring C (green balls) atoms of $C_{sp}{\equiv}C_{sp}$ hybridization, with a bond length of 2.32 Å. The side view of the structure in Fig. 2(b) further shows that the strong bonding interaction induces significant buckling of graphyne, with 6 C atoms protruding by about 0.68 Å. All the adsorbed Hf atoms

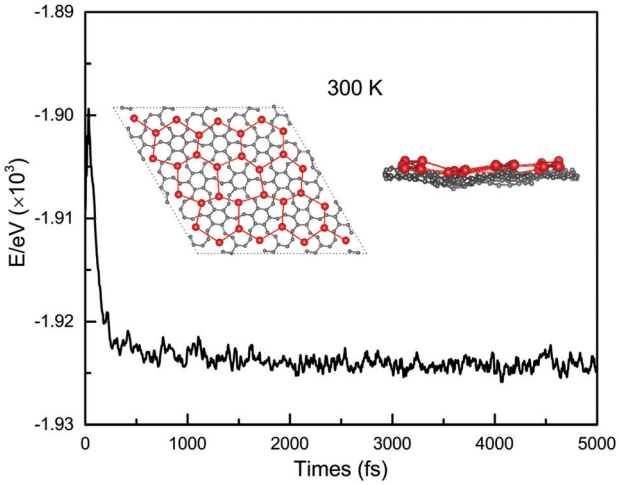

Fig. 3 Total energy fluctuations during AIMD simulations of Hf–graphyne at 300 K. The insets show snapshots at 5 ps from the 4 × 4 supercell simulation.

are 0.96 Å above the buckled C layer, forming a pretty hexagonal Hf ML. This feature makes the H1–H1 structure present high C_{v6} symmetry, which allows the formation of Dirac states. It is noticed that the nearest-neighboring distance between Hf–Hf atoms in the H1–H1 configuration is 3.98 Å, 28% larger than the Hf–Hf bond length in bulk Hf. This result means that the interaction strength among Hf atoms of the H1–H1 configuration is between the usual chemical bonding and van der Waals bonding, which may induce novel electronic properties as discussed in the following.

We now discuss the electronic properties of the H1–H1 Hf–graphyne structure. The total-energy electronic-structure calculations show that the Hf–graphyne structure favors the ferromagnetic (FM) spin ordering, with a magnetic moment of 1.03 μ_B per primitive cell. It is known that the bulk Hf is a nonmagnetic material, and the appearance of the FM state in the Hf ML indicates the existence of new physics in the 2D TM structure. The corresponding electronic band structure is further calculated. As shown in Fig. 2(c and d), the spin-up and spin-down energy bands have distinct dispersions, consistent with the feature of the FM state. An interesting finding is that three Dirac cones appear around the K point near the E_F, *i.e.*, one Dirac cone is 0.25 eV above E_F at the K point of the BZ and two Dirac cones are located adjacent to E_F around the K point. The first one is from the pure spin-up electrons (denoted as the up Dirac cone) and the remaining two are from the crossover of spin-up and spin-down electrons near the K point (denoted as up-down Dirac cones). Note that the energy bands around the K' point in the BZ are very similar to those around the K point due to the C_{v6} symmetry of the system.

To understand the origin of the three Dirac cones in Hf–graphyne, we further calculated the projected band structures onto each constituent element with different orbital symmetries (Fig. 4). One can see that the energy bands around E_F are mainly attributed to the out-of-plane d_{z^2} orbital and in-plane d_{xy/x^2-y^2} orbitals of Hf atoms, as well as the p_z orbital of C atoms. The up Dirac cone is mainly from the d_{z^2} orbital of Hf atoms, whereas the two up-down Dirac cones are attributed to the hybridization of the d_{xy/x^2-y^2} orbitals of Hf atoms and the p_z orbital of C atoms (denoted as d_{hc} orbitals) for the spin-down band and the d_{z^2} orbital of Hf atoms for the spin-up band. We have additionally calculated the spin polarized orbital projected density of states (PDOS), as shown in Fig. 4(e and f). From PDOS, one can see that energy levels near E_F are mainly contributed by the $d_{z^2/xy/x^2-y^2}$ orbitals of Hf atoms and the p_z orbital of C atoms. This result is coincident with the foregoing analysis of orbitals adjacent to E_F. It is noticed that the 2D hexagonal crystal field is expected to split the 5d orbitals of Hf atoms into three groups, *i.e.*, doubly degenerate d_{xy/x^2-y^2} orbitals, doubly degenerate $d_{yz/xz}$ orbitals, and a singly degenerate d_{z^2} orbital, all of which have energy levels around E_F (Fig. S2, ESI†). Moreover, the band structures of an isolated Hf-monolayer detached from graphyne (Fig. S2, ESI†) show a salient feature that there are Dirac bands capped with a flat band in spin-down states (Fig. S2(c), ESI†), giving rise to the so-called Kagome bands. The Dirac point mainly originates from the s orbital while the flat band is composed of d_{xy/x^2-y^2} orbitals. This interesting electronic structure is the same as in ref. 18. The physics origin of such peculiar property is that s and d_{xy/x^2-y^2} orbitals hybridize to form bonding σ and antibonding σ* states (called sd^2 hybridization) which mainly distribute in the middle of the bond, as theoretically demonstrated in ref. 18. These bond-centered states originating from sd^2 hybridization effectively transform the hexagonal symmetry of the atomic Hf lattice into the physics of the Kagome lattice. On the other hand, the p orbitals of C atoms in graphyne are divided into two groups: $p_{x/y}$ orbitals and p_z orbital. Thus it is the strong interfacial interaction, inducing the hybridizations between the d_{xy/x^2-y^2} orbitals of Hf and the p_z orbitals of C, and forming the d_{hc} orbitals with energy levels around E_F. Such orbital hybridization also affects the energy levels of the $d_{yz/xz}$ orbitals of Hf atoms due to its induced redistribution of orbital densities, which pulls the energy levels of $d_{yz/xz}$ orbitals far away from E_F, as shown in Fig. 4(e). In contrast, the d_{z^2} orbital, which does not hybridize with the in-plane orbitals, is hardly influenced by the d_{hc} hybridization, so its energy level can stay around E_F and form the Dirac cone at the $K(K')$ point. As remarked earlier, Hf–graphyne is equipped with a magnetic state. The major contributions to the magnetic moment originate from the out-of-plane d_{z^2} orbital, as represented in Fig. 4(e and f).

It is known that when the SOC effect is introduced into the Dirac sates and opens a band gap, the non-trivial topological phase can be expected in the material[7] and the Dirac states are called topological Dirac states.[38] Although SOC is a small perturbation in a crystalline solid and has little effect on the structure and energy, it may play a significant role in the electronic states near E_F of a 2D heterojunction structure. As shown in Fig. 5(a), a very large band gap for the spin-down electrons at the Γ point (300 meV) induced by the SOC is indeed observed. The SOC also opens sizeable band gaps on the three Dirac cones, *i.e.*, 70 meV (left) and 30 meV (right) for the two up-down Dirac cones induced by the d_{hc} orbitals, and 6 meV for the up Dirac cone originating from the d_{z^2} orbitals. The orbital

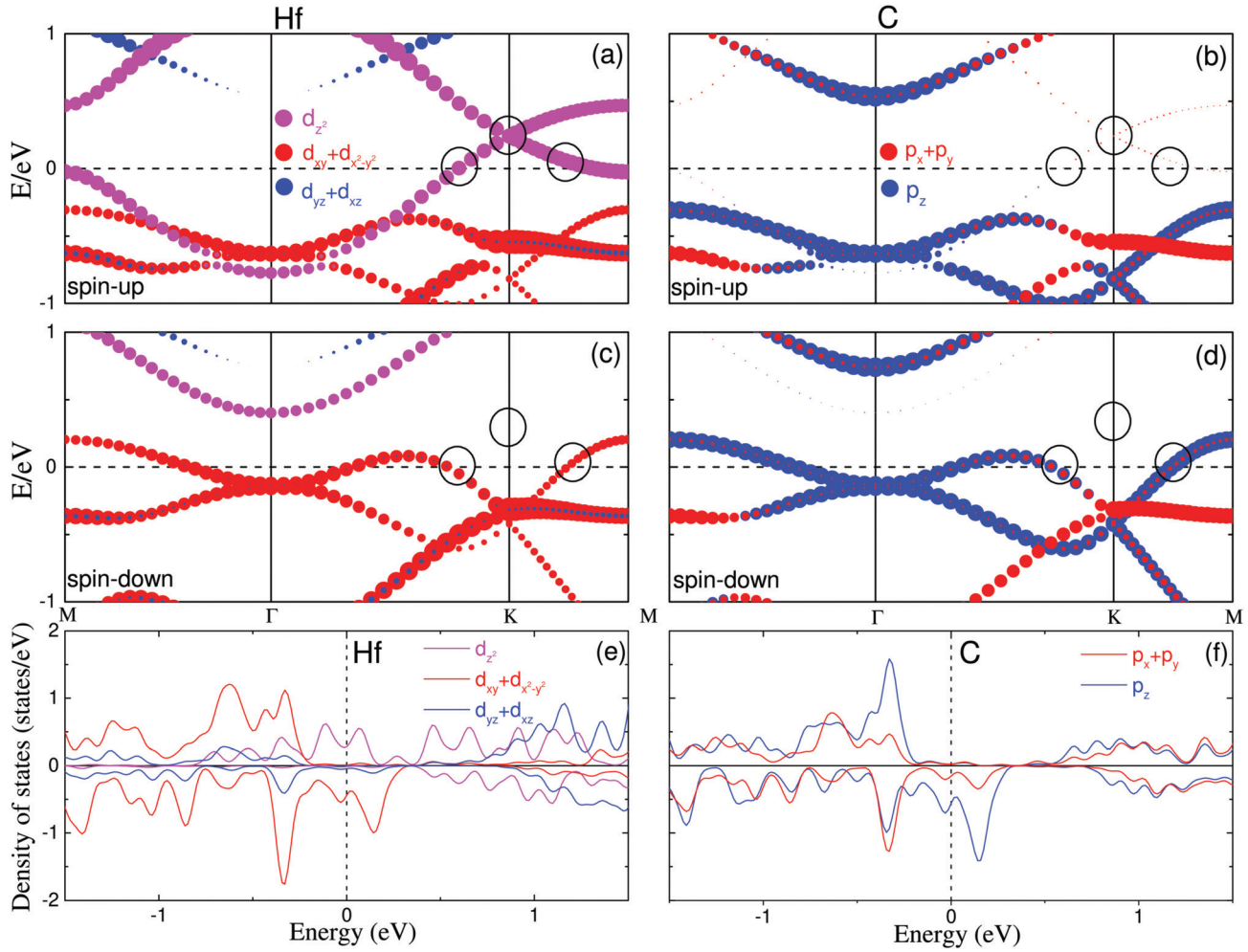

Fig. 4 Calculated band structures of Hf–graphyne projected onto Hf (a and c) and C (b and d) with different orbital symmetries for spin-up electrons (a and b) and spin-down electrons (c and d), respectively. The positions of three Dirac cones are circled by the black lines. The calculated spin polarized orbital projected density of states (PDOS) for Hf and C atoms are shown in (e) and (f), respectively.

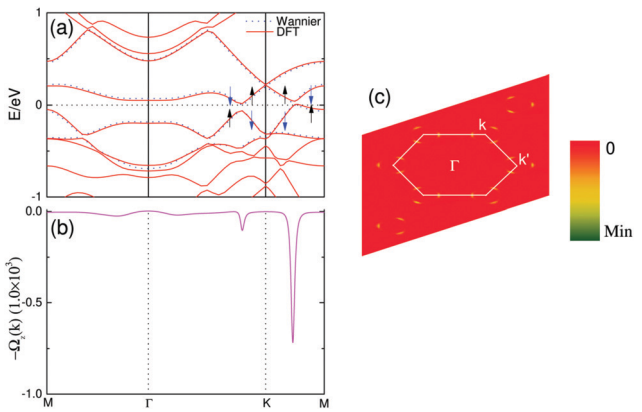

Fig. 5 (a) Calculated band structures of Hf–graphyne with spin–orbit coupling (red line) and fitted bands by MLWFs (blue dots). The spin polarizations around the Dirac cones are indicated by the arrows. (b and c) The corresponding distribution of the Berry curvature in momentum space along the high-symmetry direction (b) and two-dimensional Brillouin zone (c). All Berry curvatures are in units of Å^2.

projection analysis further shows that the band gaps of up-down Dirac cones originate from the split of energy levels for each spin-up and spin-down state at the Dirac point, different from the up Dirac cone which is purely from the spilt of the spin-up energy level. These SOC gaps are expected to originate from the combined effects of intrinsic SOC and Rashba SOC, due to the breaking of inverse symmetry in the z direction.[38–41]

Finally, we discuss the QAH effect in Hf–graphyne. With a staggered magnetic field emerging from the spin-polarized Dirac fermion and SOC, Hf–graphyne may exhibit the QAH effect featuring a nontrivial Chern number.[40,42] To calculate the Chern number of Hf–graphyne, we interpolated the spin-polarized Dirac bands based on the atom-centered MLWFs with the SOC effect turned on. As shown in Fig. 5(a), the Wannier-interpolated bands agree well with the DFT results around E_F. With the obtained MLWFs, we calculated the gauge-invariant Berry curvature $\Omega(k)$ in the momentum space

$$\Omega(k) = \sum_n f_n \Omega_n(k) \quad (2)$$

with

$$\Omega_n(k) = -2\mathrm{Im}\sum_{m\neq n}\frac{\hbar^2\langle\psi_{nk}|\,\nu_x|\psi_{mk}\rangle\langle\psi_{mk}|\,\nu_y|\psi_{nk}\rangle}{(E_m - E_n)^2} \quad (3)$$

where Ω_n is the momentum-space Berry curvature for the nth band,[43–45] E_n is the eigenvalue of the Bloch functions $|\psi_{n\kappa}\rangle$, $\nu_{x(y)}$ are the velocity operators, f_n is the Fermi–Dirac distribution function, and the summation is over all of the occupied states.

Fig. 5(b and c) show the calculated Berry curvature distribution along the high symmetry direction M–Γ–K–M and in 2D momentum space, respectively. As one can see, there are two Berry curvature peaks around each $K(K')$ point. Their positions in the BZ coincide with those of the two up-down Dirac cones, whose band gaps are opened by the SOC. This feature agrees with the conventional finding, *i.e.*, Dirac cones are expected to contribute to the Berry curvature peak and thus the nonzero Chern number with the appearance of an SOC band gap. The first Chern number C was additionally calculated by integrating the Berry curvature $\Omega(k)$ over the BZ,

$$C = \frac{1}{2\pi}\sum_n\int_{\mathrm{BZ}}\mathrm{d}^2k\Omega_n \quad (4)$$

As a result, we get $C = -3$, showing that there are three nontrivial edge states in Hf–graphyne as confirmed in Fig. S3 (ESI†). The negative value of C comes from the negative nonzero Berry curvatures (Fig. 5(b and c)). The main contribution to the Berry curvature is sharply concentrated around the two d_{hc}-ortbial Dirac cones, indicating that the main source of the anomalous Hall conductivity arises from states near the SOC gaps. On the other hand, we found that the d_{z^2}-ortbial Dirac state yields a trivial topological gap, different from the d_{hc}-orbital ones. The above results confirm that the QAH state can be realized in the 2D TM grown on graphyne, which opens a new window for the realization of the room-temperature QAH effect.

4. Conclusions

In conclusion, we have proposed a new strategy for obtaining 2D magnetic materials with topological Dirac states, *i.e.*, growing a transition-metal Hf monolayer on graphyne. We have found that the significant orbital hybridizations between Hf and C atoms in 2D materials can induce sizable magnetism and bring three Dirac cones at/around each high-symmetry $K(K')$ point in the BZ. One Dirac cone is formed by pure spin-up electrons from the d_{z^2} orbital of Hf atoms, and the remaining two Dirac cones are formed by the crossover between spin-up electrons from the d_{z^2} orbital and spin-down electrons from the hybridization of the d_{xy/x^2-y^2} orbitals of Hf atoms and the p_z orbital of C atoms. The inclusion of SOC opens up band gaps of 6 meV for the d_{z^2}-orbital Dirac cone and 70 meV and 30 meV for the remaining two Dirac cones, respectively. The Berry curvature calculations have shown that the system is topologically nontrivial with a large negative Chern number $C = -3$, which is mainly attributed to the two remaining Dirac cones. Moreover, molecular dynamics simulations show that Hf–graphyne can maintain its structural integrity up to 300 K.

Conflicts of interest

There are no conflicts to declare.

Acknowledgements

This work was supported by the National Key R&D Program of China (2018YFB0407600), the Science Fund for Distinguished Young Scholars of Hunan Province (No. 2018JJ1022) and the National Natural Science Foundation of China (No. 11604278 and 11704007).

References

1 K. S. Novoselov, A. K. Geim, S. V. Morozov, D. Jiang, Y. Zhang, S. V. Dubonos, I. V. Grigorieva and A. A. Firsov, *Science*, 2004, **306**, 666–669.
2 A. K. Geim and K. S. Novoselov, *Nat. Mater.*, 2007, **6**, 183.
3 A. H. Castro Neto, F. Guinea, N. M. R. Peres, K. S. Novoselov and A. K. Geim, *Rev. Mod. Phys.*, 2009, **81**, 109–162.
4 W.-B. Zhang, Z.-B. Song and L.-M. Dou, *J. Mater. Chem. C*, 2015, **3**, 3087–3094.
5 M. Z. Hasan and C. L. Kane, *Rev. Mod. Phys.*, 2010, **82**, 3045–3067.
6 X.-L. Qi and S.-C. Zhang, *Rev. Mod. Phys.*, 2011, **83**, 1057–1110.
7 C. L. Kane and E. J. Mele, *Phys. Rev. Lett.*, 2005, **95**, 226801.
8 S. Cahangirov, M. Topsakal, E. Aktürk, H. Şahin and S. Ciraci, *Phys. Rev. Lett.*, 2009, **102**, 236804.
9 M. Ezawa, *J. Phys. Soc. Jpn.*, 2015, **84**, 121003.
10 C. C. Liu, W. Feng and Y. Yao, *Phys. Rev. Lett.*, 2011, **107**, 076802.
11 Y. Xu, B. Yan, H. J. Zhang, J. Wang, G. Xu, P. Tang, W. Duan and S. C. Zhang, *Phys. Rev. Lett.*, 2013, **111**, 136804.
12 H. Zhao, C. W. Zhang, W. X. Ji, R. W. Zhang, S. S. Li, S. S. Yan, B. M. Zhang, P. Li and P. J. Wang, *Sci. Rep.*, 2016, **6**, 20152.
13 M. Zhou, W. Ming, Z. Liu, Z. Wang, P. Li and F. Liu, *Proc. Natl. Acad. Sci. U. S. A.*, 2014, **111**, 14378–14381.
14 C.-C. Liu, S. Guan, Z. Song, S. A. Yang, J. Yang and Y. Yao, *Phys. Rev. B: Condens. Matter Mater. Phys.*, 2014, **90**, 085431.
15 F. Reis, G. Li, L. Dudy, M. Bauernfeind, S. Glass, W. Hanke, R. Thomale, J. Schäfer and R. Claessen, *Science*, 2017, **357**, 287–290.
16 Z. F. Wang, Z. Liu and F. Liu, *Phys. Rev. Lett.*, 2013, **110**, 196801.
17 Z. F. Wang, N. Su and F. Liu, *Nano Lett.*, 2013, **13**, 2842–2845.
18 M. Zhou, Z. Liu, W. Ming, Z. Wang and F. Liu, *Phys. Rev. Lett.*, 2014, **113**, 236802.
19 L. Z. Zhang, Z. F. Wang, B. Huang, B. Cui, Z. Wang, S. X. Du, H. J. Gao and F. Liu, *Nano Lett.*, 2016, **16**, 2072–2075.
20 X.-L. Sheng and B. K. Nikolić, *Phys. Rev. B: Condens. Matter Mater. Phys.*, 2017, **95**, 201402.
21 Q. Li, Y. Li, Y. Chen, L. Wu, C. Yang and X. Cui, *Carbon*, 2018, **136**, 248–254.
22 G. Kresse and J. Furthmüller, *Comput. Mater. Sci.*, 1996, **6**, 15–50.
23 G. Kresse and J. Furthmüller, *Phys. Rev. B: Condens. Matter Mater. Phys.*, 1996, **54**, 11169–11186.

24 J. P. Perdew, K. Burke and M. Ernzerhof, *Phys. Rev. Lett.*, 1996, **77**, 3865–3868.
25 P. E. Blöchl, *Phys. Rev. B: Condens. Matter Mater. Phys.*, 1994, **50**, 17953–17979.
26 G. Kresse and D. Joubert, *Phys. Rev. B: Condens. Matter Mater. Phys.*, 1999, **59**, 1758–1775.
27 J. Heyd, G. E. Scuseria and M. Ernzerhof, *J. Chem. Phys.*, 2003, **118**, 8207–8215.
28 J. Heyd, G. E. Scuseria and M. Ernzerhof, *J. Chem. Phys.*, 2006, **124**, 219906.
29 H. J. Monkhorst and J. D. Pack, *Phys. Rev. B: Condens. Matter Mater. Phys.*, 1976, **13**, 5188–5192.
30 A. A. Mostofi, J. R. Yates, Y.-S. Lee, I. Souza, D. Vanderbilt and N. Marzari, *Comput. Phys. Commun.*, 2008, **178**, 685–699.
31 A. A. Mostofi, J. R. Yates, G. Pizzi, Y.-S. Lee, I. Souza, D. Vanderbilt and N. Marzari, *Comput. Phys. Commun.*, 2014, **185**, 2309–2310.
32 Q. Wu, S. Zhang, H.-F. Song, M. Troyer and A. A. Soluyanov, *Comput. Phys. Commun.*, 2018, **224**, 405–416.
33 Y. Jiao, A. Du, M. Hankel, Z. Zhu, V. Rudolph and S. C. Smith, *Chem. Commun.*, 2011, **47**, 11843–11845.
34 K. Srinivasu and S. K. Ghosh, *J. Phys. Chem. C*, 2012, **116**, 5951–5956.
35 L. Li, Y. Wang, S. Xie, X.-B. Li, Y.-Q. Wang, R. Wu, H. Sun, S. Zhang and H.-J. Gao, *Nano Lett.*, 2013, **13**, 4671–4674.
36 J. He, S. Y. Ma, P. Zhou, C. X. Zhang, C. He and L. Z. Sun, *J. Phys. Chem. C*, 2012, **116**, 26313–26321.
37 M. Chen and M. Weinert, *Phys. Rev. B: Condens. Matter Mater. Phys.*, 2018, **98**, 245421.
38 C. L. Kane and E. J. Mele, *Phys. Rev. Lett.*, 2005, **95**, 146802.
39 C.-C. Liu, H. Jiang and Y. Yao, *Phys. Rev. B: Condens. Matter Mater. Phys.*, 2011, **84**, 195430.
40 P. Li, X. Li, W. Zhao, H. Chen, M.-X. Chen, Z.-X. Guo, J. Feng, X.-G. Gong and A. H. MacDonald, *Nano Lett.*, 2017, **17**, 6195–6202.
41 Z. Qiao, S. A. Yang, W. Feng, W.-K. Tse, J. Ding, Y. Yao, J. Wang and Q. Niu, *Phys. Rev. B: Condens. Matter Mater. Phys.*, 2010, **82**, 161414.
42 M. Ezawa, *Phys. Rev. Lett.*, 2012, **109**, 055502.
43 D. J. Thouless, M. Kohmoto, M. P. Nightingale and M. den Nijs, *Phys. Rev. Lett.*, 1982, **49**, 405–408.
44 M.-C. Chang and Q. Niu, *Phys. Rev. B: Condens. Matter Mater. Phys.*, 1996, **53**, 7010–7023.
45 Y. Yao, L. Kleinman, A. H. MacDonald, J. Sinova, T. Jungwirth, D.-S. Wang, E. Wang and Q. Niu, *Phys. Rev. Lett.*, 2004, **92**, 037204.

